Size- and temperature-dependent bending rigidity of graphene using modal analysis

Sajadi, Banafsheh; van Hemert, Simon; Arash, Behrouz; Belardinelli, Pierpaolo; Steeneken, Peter G.; Alijani, Farbod

DOI
10.1016/j.carbon.2018.06.066

Publication date
2018

Document Version
Final published version

Published in
Carbon

Carbon 139 (2018) 334–341

Contents lists available at ScienceDirect

Carbon

journal homepage: www.elsevier.com/locate/carbon

Size- and temperature-dependent bending rigidity of graphene using modal analysis

Banafsheh Sajadi [a], Simon van Hemert [a], Behrouz Arash [b], Pierpaolo Belardinelli [a], Peter G. Steeneken [a, c], Farbod Alijani [a, *]

[a] Department of Precision and Microsystems Engineering, Faculty of Mechanical, Maritime and Materials Engineering, Delft University of Technology, 2628 CD, Delft, the Netherlands
[b] Department of Structural Engineering, Faculty of Civil Engineering and Geosciences, Delft University of Technology, 2628 CN, Delft, the Netherlands
[c] Kavli Institute of Nanoscience, Faculty of Applied Sciences, Delft University of Technology, 2628 CJ, Delft, the Netherlands

ARTICLE INFO

Article history:
Received 26 March 2018
Received in revised form
26 June 2018
Accepted 27 June 2018
Available online 29 June 2018

Keywords:
Graphene
Bending rigidity
Brownian motion
Characterization
Multi-modal approach
Molecular dynamics

ABSTRACT

The bending rigidity of two-dimensional (2D) materials is a key parameter for understanding the mechanics of 2D NEMS devices. The apparent bending rigidity of graphene membranes at macroscopic scale differs from theoretical predictions at micro-scale. This difference is believed to originate from thermally induced dynamic ripples in these atomically thin membranes. In this paper, we perform modal analysis to estimate the effective bending rigidity of graphene membranes from the frequency spectrum of their Brownian motion. Our method is based on fitting the resonance frequencies obtained from the Brownian motion in molecular dynamics simulations, to those obtained from a continuum mechanics model, with bending rigidity and pretension as the fit parameters. In this way, the effective bending rigidity of the membrane and its temperature and size dependence, are extracted, while including the effects of dynamic ripples and thermal fluctuations. The proposed method provides a framework for estimating the macroscopic mechanical properties in other 2D nanostructures at finite temperatures.

1. Introduction

The exceptional mechanical properties of graphene have made it a promising candidate for the next generation of 2D nano-resonators with potential applications in pressure sensing [1,2], mass sensing [3,4], and electronics [5–7]. A proper understanding of the mechanics of this material is not only of fundamental interest but also a key step towards the development of new devices. Therefore, the elastic properties of graphene have been investigated in many theoretical and experimental studies [8–13].

The bending rigidity of graphene, however, is still far from being well-understood and compared to its Young's modulus, it is much less investigated. This is due to the fact that for a single atom thick membrane, this parameter is not determined by layer thickness, but by the bending-induced changes in interactions between electron orbitals. In fact, due to its low bending rigidity, as compared to the limit of the continuum plate theories, graphene is commonly assumed to have a membrane-like behavior with a negligible (zero) bending rigidity [11,12].

Direct measurement of bending rigidity has therefore been challenging for mono-layer graphene, as well as other atomically thin membranes. The mostly cited experimental value of 1.2eV was derived from the phonon spectrum of graphite [14]. In another study, Lindahl et al. [10] proposed a framework for extracting the bending rigidity of a graphene membrane from the snap-through behavior of its buckled configuration. Based on the proposed method, the authors reported a bending rigidity of 7.1eV with a large uncertainty of (-3eV to +4eV) for mono-layer graphene. In a more recent study, Blees et al. [15], measured effective bending rigidity of $10^3 - 10^4$ eV. In this study, the authors have suggested significant effects of thermal fluctuations as well as static wrinkles on the obtained large bending rigidity.

On the other hand, many studies have investigated the theoretical limit of the bending rigidity of mono-layer graphene [16–18]. The theoretical calculations of the bending rigidity for mono-layer graphene have a large range of 0.69eV–0.83eV by models using the Brenner potentials [19], 1.4eV–1.6eV by semi-analytical and density functional theories [18,20,21], and 0.360eV–2.385eV by molecular mechanics simulations, varying

* Corresponding author.
E-mail address: f.alijani@tudelft.nl (F. Alijani).

https://doi.org/10.1016/j.carbon.2018.06.066

with size and aspect ratio of the membrane [22]. It has been reported that bond-angle effects and the bond associated with the dihedral angles are in fact the two dominant sources of the apparent finite bending rigidity of graphene membranes [18]. In addition to these effects, Roldan et al. [23] suggested that the bending rigidity of graphene at finite temperatures is also highly influenced by the thermodynamics. In Ref. [23], the authors used a self-consistent theory of elastic membranes [24] and proposed a thermodynamical approximation for the effective wave vector dependent bending rigidity (κ) in formation of dynamic ripples:

$$\kappa = \kappa_0 + k_B T A (q_0/q)^{\eta}, \tag{1}$$

where T is the temperature, k_B is the Boltzmann constant, $\kappa_0 = 1eV$, $A = 5.9T^{(\eta/2-1)}$, $\eta = 0.85$, and q is the wave number associated with dynamic ripples. These ripples are shown to be large enough to affect the effective macroscopic mechanical properties of atomically thin membranes and ribbons [13,23,25–30]. Moreover, $q_0 = 2\pi\sqrt{E_{2D}/\kappa_0}$ [23,28], where E_{2D} is the lateral stretching stiffness of the membrane.

In this paper, we propose a novel approach based on modal analysis for direct estimation of the macroscopic bending rigidity of graphene membranes. Our method incorporates the effect of Brownian motion and the resulting ripples on the bending rigidity. We determine a single bending rigidity and pretension with which our model can accurately reproduce up to 10 vibration modes and natural frequencies obtained from atomistic simulations. Furthermore, we show that our obtained bending rigidity can be best fitted with an effective wave number $q_{\text{eff}} = \pi/R$, to Equation (1), where R is the radius of the membrane.

The proposed approach for determining the bending rigidity of graphene is outlined as follows: In Section 2, we derive a continuum mechanics (CM) model for the resonance frequencies of a prestressed circular graphene membrane as a function of its pretension and bending rigidity. In Section 3, we employ Molecular Dynamics (MD) simulations to model the Brownian motion in the graphene membrane at finite temperatures. The natural frequencies of the MD model are obtained by applying Fast Fourier Transform (FFT) to the time signals extracted from MD. Finally, in Section 4, by fitting the resonance frequencies obtained from the Brownian motion, to those obtained from CM, the effective bending rigidity is extracted. Moreover, in Section 5, the effects of different temperatures and radii of the membrane on the bending rigidity are discussed, and the results are compared to Equation (1).

2. Governing equations

In this section, we propose a model for obtaining the resonance frequencies of a prestressed circular graphene membrane as a function of its pretension and bending rigidity. In addition to the symmetry, the choice of circular drums is because 2D NEMS devices with circular shape yield better structural flexibility compared to other geometries and have no corners or sharp edges that can induce high residual stresses in practical applications [31]. However, it should be mentioned that the bending rigidity of graphene membranes, particularly at small scales, is expected to depend on the shape of the membrane as well [22].

We obtain the equations of motion by using the von Kármán plate theory [32] and by following Lagrangian approach. In our formulation, bending rigidity (κ) and the pretension (n_0) of the membrane are considered to be unknown parameters that will be calibrated by means of MD simulations. In this approach, we approximate the transverse displacement component by a superposition of a finite number of suitably chosen basis functions:

$$w(t,r,\theta) = \sum_{i=1}^{n} q_i(t)\Phi_i(r,\theta), \tag{2}$$

where q_i are the time dependent generalized coordinates and Φ_i are the admissible shape functions. Here, the vibration modes of a circular membrane (with negligible bending stiffness) are employed as the shape functions [33]:

$$W_{mn}(r,\theta) = J_m\left(\beta_{mn}\frac{r}{R}\right)\cos(m\theta), \quad m = 0,1,\ldots n = 1,2,\ldots \tag{3}$$

where r and θ are polar coordinates, R is the radius of the membrane, J_m is the m^{th} order Bessel function of the first kind, and β_{mn} is the n^{th} root of the Bessel function. The chosen subset for the spectral projection is $\Phi = [W_{01}, W_{11}, W_{21}, W_{02}, W_{31}, W_{12}, W_{41}, W_{22}, W_{03}, W_{51}]$ which correspond to the modes with the 10 lowest frequencies, and it will be shown that these are sufficient for obtaining a converged bending rigidity.

Next, in order to form the Lagrange equations, the total potential energy and kinetic energy of the system shall be obtained. In linear vibrations, the total strain energy of a circular membrane with bending rigidity consists of two terms: (i) the membrane term which is the stretching potential energy of a classical plate where the nonlinear in-plane displacement due to transverse deflection is neglected and only the terms due to the pretension (n_0) are included, and (ii) the bending term which is similar to the bending potential of a classical Kirchhoff plate in small deflections and rotations [32]. Therefore, the potential energy can be obtained in terms of transverse displacement component and its derivatives as:

$$\begin{aligned} U = \frac{1}{2}\kappa \int_0^{2\pi}\int_0^{R}\Bigg(&\left(\nabla^2 w\right)^2 - 2(1-\nu)\frac{\partial^2 w}{\partial r^2}\left(\frac{1}{r}\frac{\partial w}{\partial r} + \frac{1}{r^2}\frac{\partial^2 w}{\partial \theta^2}\right) \\ &+2(1-\nu)\left(\frac{1}{r}\frac{\partial^2 w}{\partial r \partial \theta} - \frac{1}{r^2}\frac{\partial w}{\partial \theta}\right)^2\Bigg) \\ &+\frac{1}{2}n_0\int_0^{2\pi}\int_0^{R}\left(\left(\frac{\partial w}{\partial r}\right)^2 + \left(\frac{1}{r}\frac{\partial w}{\partial \theta}\right)^2\right) r\,\mathrm{d}r\mathrm{d}\theta, \end{aligned} \tag{4}$$

where ν is the Poisson's ratio. Assuming temperature independent material properties, the pretension due to a thermal strain can be derived as [32]:

$$n_0 = -\frac{\alpha E_{2D}}{1-\nu}\Delta T, \tag{5}$$

in which E_{2D} is the lateral stretching stiffness of the membrane, α is the thermal expansion coefficient, and ΔT is the temperature change in the membrane. The kinetic energy of the membrane with a density of ρ and a thickness of h is given by

$$K = \frac{1}{2}\rho h \int_0^{2\pi}\int_0^{R} \dot{w}^2\, r\,\mathrm{d}r\mathrm{d}\theta. \tag{6}$$

As a consequence, the Lagrangian of the system ($L = K - U$) can be formulated as a function of the unknown parameters q_i, n_0, and κ, as well as the known variables R, h, E_{2D} and ν. Using Lagrange equations, a set of n equations describing the motion of the membrane in terms of q_i is obtained. The set of equations of motion can be expressed in the matrix form as:

$$\overline{\overline{\mathbf{M}}}\ddot{\mathbf{q}} + \overline{\overline{\mathbf{K}}}\mathbf{q} = 0, \tag{7}$$

where $\overline{\overline{\mathbf{K}}}$ and $\overline{\overline{\mathbf{M}}}$ are the equivalent stiffness and mass matrices, respectively, in which $k_{ij} = \frac{\partial^2 U}{\partial q_i \partial q_j}$ and $m_{ij} = \frac{\partial^2 K}{\partial \dot{q}_i \partial \dot{q}_j}$. Moreover, $\mathbf{q}$ is the vector comprising time dependent generalized coordinates. The resonance frequencies can be directly determined from the characteristic equation of this system (i.e. $\det(\overline{\overline{\mathbf{M}}}^{-1}\overline{\overline{\mathbf{K}}} - \bar{\bar{\mathbf{I}}}\omega^2) = 0$).

It should be noted that the stiffness matrix ($\overline{\overline{\mathbf{K}}}$), and hence the obtained resonance frequencies (ω_i^{CM}) will be functions of the pretension (n_0) and bending rigidity (κ). These frequencies are independent of the value of the elastic modulus, since, the elastic modulus only affects the nonlinear dynamics of the membrane at large amplitudes [12] and not the linear response.

3. Numerical implementation

In order to perform MD simulations, we use LAMMPS software [34]. In this software, the equations of motion are integrated using the velocity-Verlet integrator algorithm, with a time-step of 1 fs. The simulations are performed for a circular, flat, mono-layer graphene sheet with a radius of 1–10 nm. The atoms in this structure are ordered in a hexagonal grid with an inter-atomic distance of 1.42 Å (see Fig. 1a). The forces between atoms are described by the Tersoff potential, which is commonly used for modeling the atomic interactions in diamond, graphite, and graphene [17].

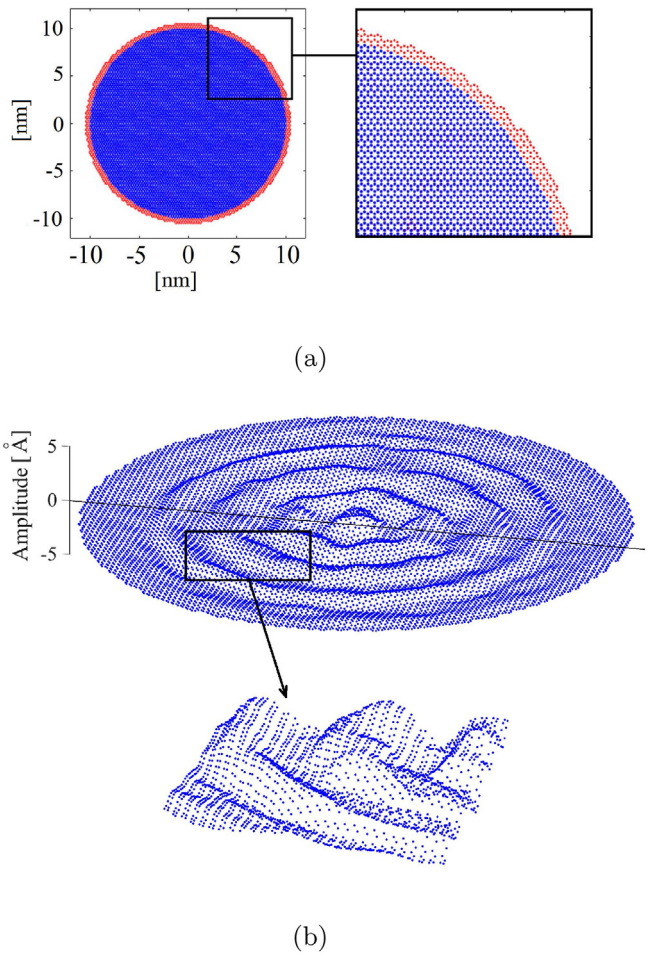

Fig. 1. The schematics of MD model. a) The circular, flat, mono-layer graphene sheet with a radius of 10 nm (blue dots), and three rows of atoms along the boundary at which the degrees of freedom is restricted (red dots). b) A snapshot of the Brownian motion of the membrane with radius of $R = 10$ nm, and $T = 300$ K. (A colour version of this figure can be viewed online.)

Since the initial position of the atoms may not exactly correspond to equilibrium or the minimum potential state, the system is relaxed by minimizing the total potential energy. The minimization is performed by the Polak-Ribiere conjugate gradient algorithm [35]. The iterations are terminated when the energy is less than 1×10^{-10} eV or when the forces are less than 1×10^{-10} eV/Å. While relaxing the system, the out of plane motion is inhibited, to prevent curling of the membrane. After the relaxation, the edge is fully clamped by restricting all the translational degrees of freedom of three rows of atoms along the boundary.

Next, the system is allowed to equilibrate in the constant volume and constant temperature ensemble (NVT) using the Nose-Hoover thermostat algorithm [36]. In this stage, the Nose-Hoover thermostat guarantees the Maxwell-Boltzmann velocity distribution, while the damping parameter is 20 fs, which is sufficient in the stable temperature conditions. The algorithm is performed for 50 ps (i.e. 50000 time-steps) to ensure a stable temperature is achieved. The results of our simulations show that a 50 ps of NVT simulation is sufficient to equilibrate the largest membrane (20-nm diameter graphene) for our highest simulation temperature. During thermalization, the boundaries of the membrane are fixed. This means the membrane will be tensioned, as a result of the negative thermal expansion of graphene [37,38]. Finally, the vibration response is studied in an energy conserving ensemble (NVE).

After the desired temperature is achieved, the thermal fluctuations of the graphene membrane are monitored for 20ns. The atoms coordinates are saved every 0.5 ps (i.e. 500 time-steps), which corresponds to approximately 20 points per vibration period of the fifth resonance of a graphene membrane with a radius of 10 nm in 300 K. To avoid under-sampling, the coordinates of the atoms are saved every 0.1 ps for membranes with radii of smaller than 3 nm. The MD simulations are repeated for 4–6 times for each combination of temperature and radius. Fig. 1b, shows one snapshot of the Brownian motion of a graphene membrane with a radius of 10 nm at $T = 300$ K. The dynamic ripples due to thermal fluctuations can be clearly observed in this figure.

The time response of the position of an atom in the center of the membrane due to these thermal fluctuations over time is shown in Fig. 2. It can be observed that the range of the deflection at the center of the membrane is in the order of graphene's thickness (0.335 nm). Thus, graphene at room temperature behaves as a dynamically corrugated plate that has a corrugation amplitude similar to its thickness. This shows the importance of including thermal fluctuations in the estimation of graphene's mechanical properties, and also provides a mechanism by which the effective bending rigidity of graphene depends on temperature.

It should be mentioned that the amplitude of thermal fluctuation even at high temperatures is relatively small which ensures that the resonance frequencies are not largely affected by nonlinearities. In order to observe nonlinear effects, large amplitude vibrations are needed which would require imposing a large initial velocity/displacement to the membrane [39,40]. However, this amplitude dependent frequency in graphene has been shown to be eventually damped to the linear frequencies of the membrane during thermalization [41]. Since in our work, the idea is to obtain linear frequencies, we only look into the final stabilized condition that includes the natural frequencies that are required to obtain a converged bending rigidity.

By applying FFT to the obtained MD time signal, the natural frequencies of the membrane are obtained. The FFT is performed on

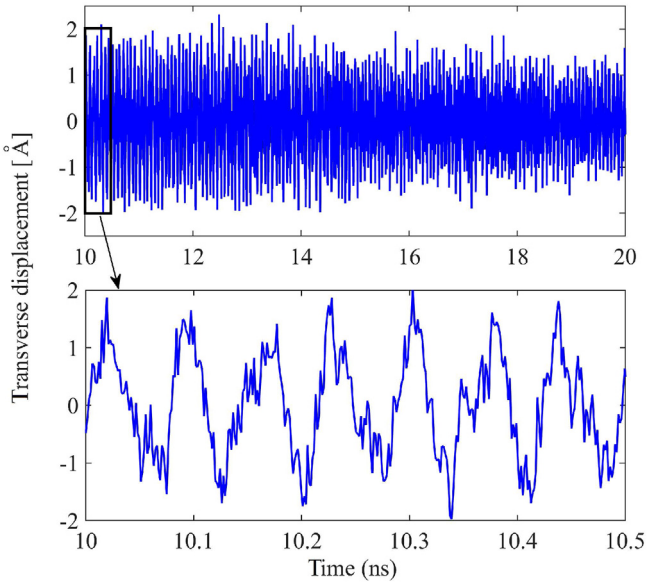

Fig. 2. Transverse position of the center atom over time, while $R = 10$ nm, and $T = 300$ K. (A colour version of this figure can be viewed online.)

the transverse displacement of atoms (orthogonal to the surface of the pristine graphene sheet), and then, the average of the FFT spectra of all atoms is considered as the frequency spectrum [42,43]. Fig. 3a shows the frequency spectrum obtained by averaging the FFT responses of the time signals of the atoms.

4. Identification technique

To identify resonance frequencies from MD simulations, the time response shall be filtered with respect to the associated modes. This filtering is performed by using the orthogonality of vibration modes, i.e. by projecting the time response on a certain mode shape [33]. This projection shall be performed via a dot product between the snap-shots of the MD transverse motion and the vector describing the vibration modes at the position of all atoms. The analytic solutions for the mode shapes of a circular clamped membrane are used for the vibration modes. For each of the mode shapes, a time-trace of the resulting dot product is determined and an FFT is applied. Fig. 3b shows the filtered frequency response of the first few modes of vibrations, indicated in different colors. By determining the peak frequency of each of the mode shapes, the first 10 resonance frequencies (i.e. ω_i^{MD}) of the MD model are determined.

Next, the resonance frequencies from CM (i.e. $\omega_i^{CM}(\kappa, n_0)$) is numerically fitted to the obtained set of resonance frequencies from MD (i.e. ω_i^{MD}). The fitting is performed by a least squares method and using κ and n_0 as fit parameters. The squared normalized error of N resonance frequencies between the two methods is minimized, where the error is defined as:

$$e = \sqrt{\frac{\sum_{i=1}^{N}\left(\frac{\omega_i^{MD}-\omega_i^{CM}(\kappa,n_0)}{\omega_i^{CM}}\right)^2}{N}}, \tag{8}$$

It shall be noted that mathematically, only two resonance frequencies are needed to determine κ and n_0, since it involves solving 2 equations with 2 unknowns. However, retaining higher modes is necessary to increase the accuracy because the radius of curvature of the membrane at higher frequency modes is relatively smaller, and therefore, the associated resonance frequencies are more sensitive to the bending rigidity. Moreover, by employing a higher number of degrees of freedom, one can assure that the model in (7) can better describe the dynamic ripples due to Brownian motion.

The error between the natural frequencies obtained via CM and MD models decreases by including higher modes in the fitting process and leads to a converged value for the bending rigidity. Fig. 4 shows the normalized error (e) obtained from Equation (8), as a function of the fitting parameters. This figure confirms that including higher modes in the fitting process decreases the surface area of the minimum error, and leads to a more accurate bending rigidity. These graphs clearly show the necessity of incorporating multiple modes in the approximation in order to reach a converged solution.

5. Results and discussion

The convergence of the bending rigidity and pretension versus the number of modes retained in the fitting procedure is shown in Fig. 5a and Fig. 5b, respectively. The error bars in these figures show the standard error based on 6 simulations for each point. It is seen that, at room temperature, by including 10 natural frequencies, the solution converges to a bending rigidity of 2.7eV and the corresponding pretension due to thermal strain is obtained as 0.41 N/m. It should be mentioned that the pretension calculated explicitly from MD is neither constant nor uniform due to the nature of the Brownian motion at the atomic level. However, the average mean-value pretension obtained from MD simulations at 300 K is 0.32 N/m which is in the same range as calculated by our method.

Moreover, it can be observed from Fig. 5a that the obtained

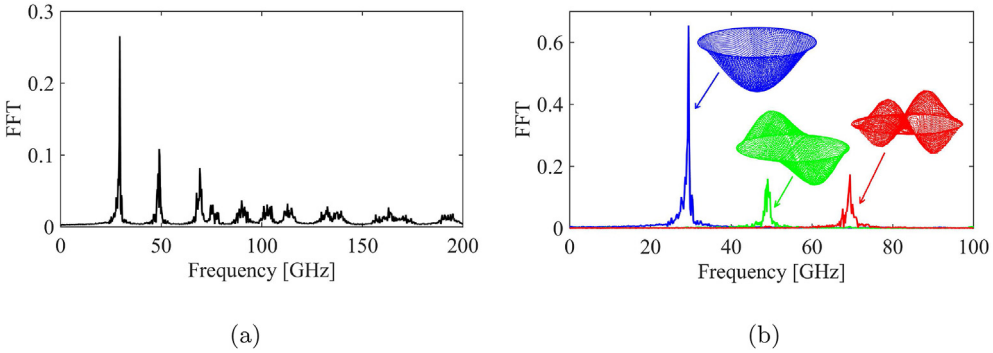

Fig. 3. a) Averaged frequency spectrum of the time response of all atoms and b) filtered frequency spectrum for the first 3 modes, while $R = 10$ nm, and $T = 300$ K. (A colour version of this figure can be viewed online.)

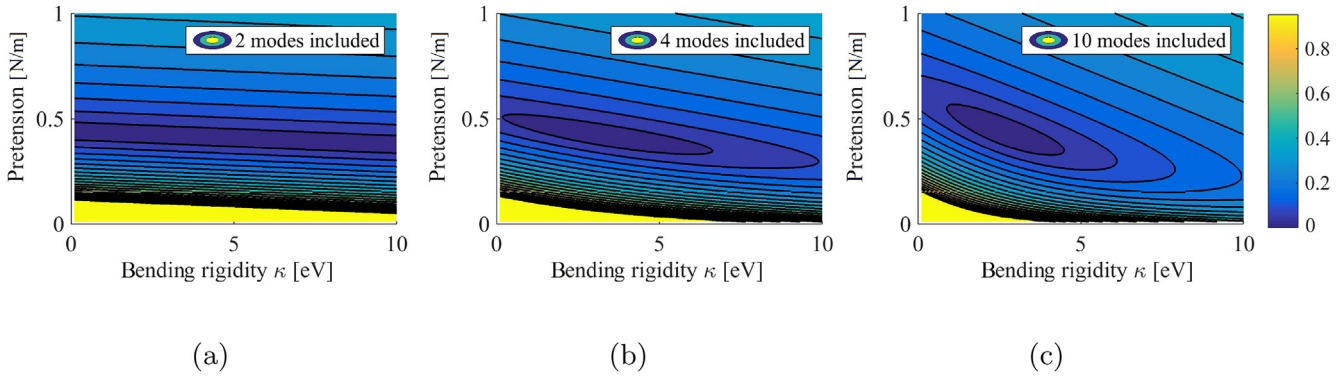

Fig. 4. The normalized error (e) as a function of the fitting parameters κ and n_0, when including a) $N = 2$, b) $N = 4$, and c) $N = 10$ frequencies, while $R = 10$ nm, and $T = 300$ K. (A colour version of this figure can be viewed online.)

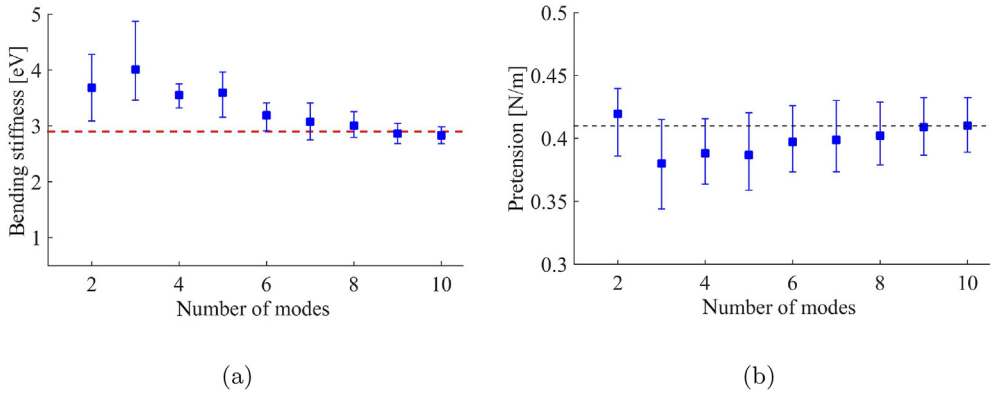

Fig. 5. a) The obtained bending rigidity κ as a function of the number of frequencies in the fitting process (blue dots) and the approximated one with $q_{\text{eff}} = \pi/R$ (red dashed line) from Equation (1) [23], and b) The obtained pretension n_0 as a function of the number of frequencies in the fitting process (blue dots) converging to a pretension of 0.41 N/m (black dashed line), for $R = 10$ nm at $T = 300$ K. (A colour version of this figure can be viewed online.)

effective bending rigidity is converging to the bending rigidity obtained by Equation (1) [23] when using an effective wave number $q_{\text{eff}} = \pi/R$. It should be noted that q_{eff} is found between discrete wave numbers that fit in the membrane. The obtained value of κ and q_{eff} are not only affected by the simultaneous fit of 10 modes with different wavelengths, but also depend on the circular geometry of the drum.

The normalized error between the obtained resonance frequencies using the proposed model with the optimized parameters and those of MD simulations are shown in Fig. 6. As it can be observed, by using only 2 modes in the fitting process, the error between the higher frequencies is relatively large. By using 10 modes, the error between the frequencies of two methods will be less than 5%, which stresses the importance of retaining higher modes of vibrations in the identification process. The ratio between the first 10 resonance frequencies and the fundamental frequency ($\omega_1 = 28.8GHz$) for one set of simulations are shown in Fig. 7. For comparison, the results of associated MD simulations and those

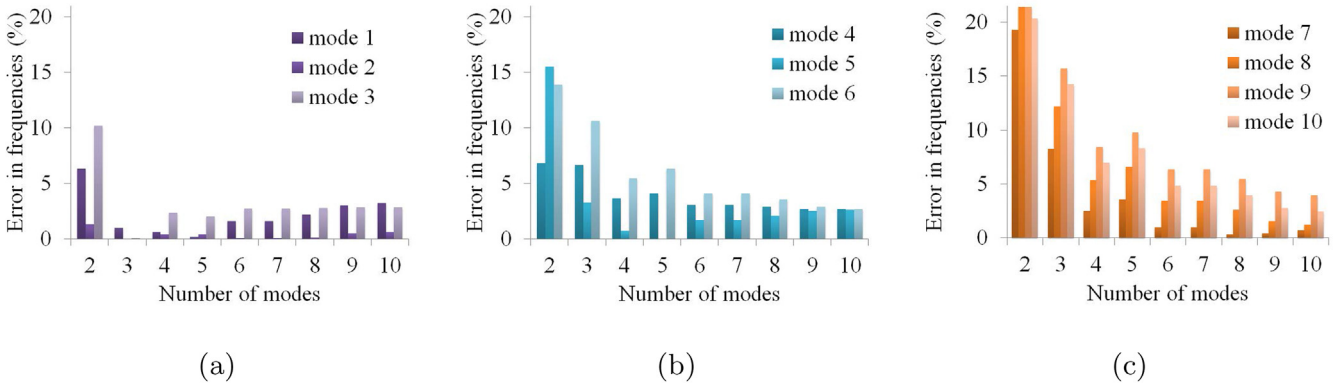

Fig. 6. The normalized error between the obtained resonance frequencies using the proposed model with the optimized parameters and those of MD simulations in percentage $\left(\left|\frac{\omega_i^{CM}-\omega_i^{MD}}{\omega_i^{MD}}\right| \times 100\right)$. (A colour version of this figure can be viewed online.)

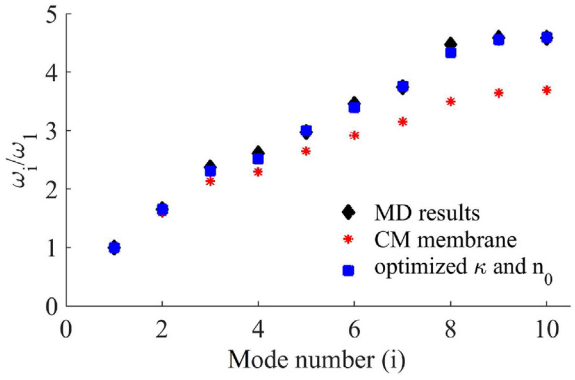

Fig. 7. The normalized natural frequencies versus the mode number, obtained from MD, the proposed model with the optimized parameters ($n_0 = 0.41N/m =$ and $\kappa = 2.7eV$), and classical membrane theory where $\kappa = 0$, for $R = 10$ nm at $T = 300$ K. (A colour version of this figure can be viewed online.)

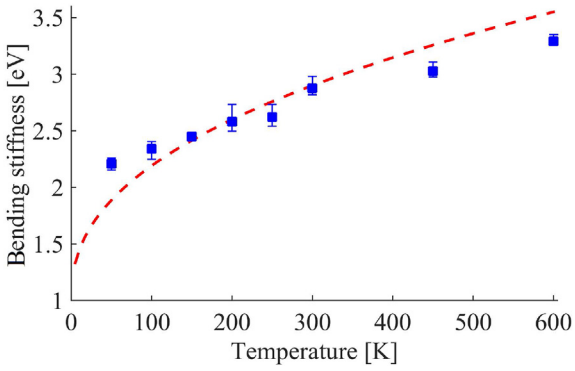

Fig. 8. The obtained bending rigidity κ (blue dots), and the approximated one with $q_{eff} = \pi/R$ (red dashed line) from Equation (1) [23], as a function of the temperature, for $R = 10$ nm. (A colour version of this figure can be viewed online.)

obtained from a classical membrane model (with zero bending rigidity) are also plotted in this figure. As can be observed, by using a single optimized value for pretension and bending rigidity, our CM model can very well reproduce all the 10 natural frequencies of the MD model, while it is clear that a membrane model that neglects the bending rigidity of graphene cannot capture the observed dynamic behavior, especially for the higher resonance modes.

Furthermore, using the proposed method, the temperature, and size dependence of the bending rigidity can be studied. In this regard, Fig. 8 shows the obtained bending rigidity as a function of temperature. Included in the figure is also the bending rigidity obtained from Equation (1) with $q_{eff} = \pi/R$. As can be seen, both methods predict an increase in the bending rigidity with increasing temperature. As it was mentioned before, the increase of bending rigidity of membranes with a crystalline and hexatic order has been previously predicted by Ref. [24]. In fact, it has been shown that the stretching energy of membranes due to thermalization drastically increases the effective bending rigidity at long wavelengths. Therefore, if we fix the boundaries before thermalization, and let the membrane to be stretched due to its negative thermal expansion, this stretching can directly result in an increase of bending stiffness. As such, if during the thermalization process, the boundary condition is eliminated and the graphene membrane is allowed to shrink, the bending rigidity will monotonically reduce with temperature [44,45]. Therefore, the boundary condition is also influential in the apparent bending rigidity of the membrane. It shall be also noted that for very high temperatures, the thermal softening due to short wavelength undulations can dominate stiffening effects, and therefore, it is expected that bending rigidity converges or even decreases at such thermal condition [24].

The increase in the bending rigidity can be also explained by the entropic effects in graphene. In fact, graphene's bending rigidity resembles an entropic spring, like a rubber band, in which entropy and thermodynamics affect elasticity. In such systems, the free energy $A = U - TS$ is a sum of the internal energy U and the product of temperature T and entropy S. The external force F needed for reversible isothermal extension of such a spring is $F = dA/dx = dU/dx - TdS/dx = k(T)x$. Therefore, the effective stiffness $k(T)$ increases with temperature due to the reduction in entropy ($dS/dx < 0$) upon elongation in the spring or rubber band.

In Fig. 9a and b, we report the bending rigidity for different radii of the membrane for temperatures of 100 and 300 K. It can be seen that the bending rigidity increases monotonically with the radius of the membrane, and it fits Equation (1) when $q_{eff} = \pi/R$. It should be noted that Equation (1) suggests a monotonic increase in the bending rigidity of the membrane with radius and temperature with no convergence. But extrapolating the formula for very large graphene membranes yields large numbers whose correctness is hard to prove or trust. At the scale at hand, we do not observe any convergence of bending rigidity either. Additional simulations performed on a 20 nm radius membrane at 300 K also gave a similar trend of increase and an equivalent bending rigidity of 3.9eV.

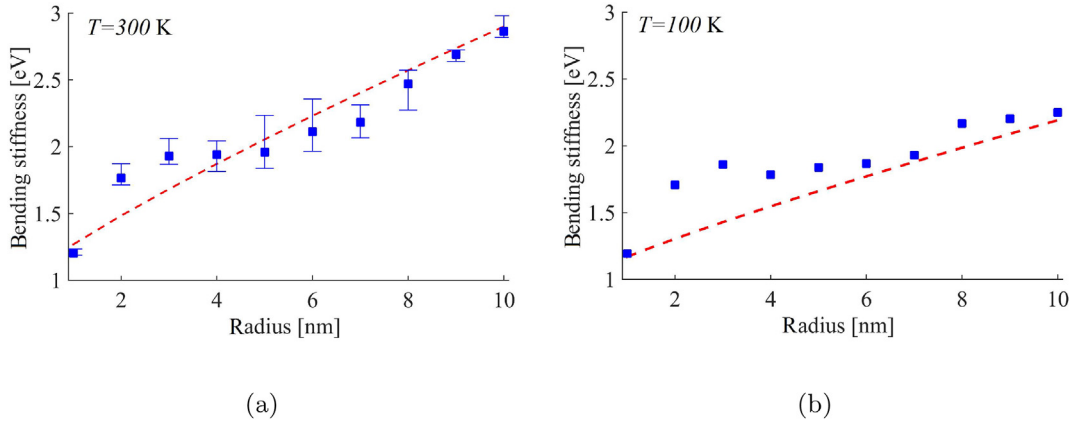

Fig. 9. The obtained bending rigidity κ (dots) and the approximated one with $q_{eff} = \pi/R$ (dashed line) from Equation (1) [23], at a) $T = 300$ K and b) $T = 100$ K. (A colour version of this figure can be viewed online.)

Moreover, the obtained trend in the size dependency (i.e. the monotonic increase with size) is in agreement with the molecular mechanics simulations of the microscopic temperature-independent bending rigidity for rectangular membranes [22]. This size dependence can be attributed to two main reasons: (i) at small scales the atoms are more bounded for free thermal fluctuations and therefore, they appear as relatively less dynamic as compared to larger scales; and (ii) at small scales the macroscopic and microscopic bending rigidities are physically non-distinguishable. As a result, our obtained bending rigidity at $R = 1$ nm is close to the microscopic temperature-independent values of 1.4eV–1.6eV [18,20–22,28].

6. Conclusions

In conclusion, we used modal analysis for direct estimation of the macroscopic bending rigidity of graphene membranes. The current work confirms that the bending rigidity in graphene membranes depends on the temperature and membrane size. Moreover, our obtained bending rigidity at small scales is in agreement with the size-dependent renormalized bending rigidity predicted by the statistical mechanics of elastic membranes with a crystalline or hexatic order. Our method is not only suitable for obtaining the bending rigidity of graphene but is also useful for characterization of other nano-materials, while incorporating thermal fluctuations.

Acknowledgements

We acknowledge productive discussions with Y.M. Blanter from TU Delft and M. Katsnelson from Radboud University. BS and FA further acknowledge the financial support from TU Delft, 3mE cohesion grant NITRO.

References

[1] Robin J. Dolleman, Dejan Davidovikj, Santiago J. Cartamil-Bueno, Herre SJ. van der Zant, Peter G. Steeneken, Graphene squeeze-film pressure sensors, Nano Lett. 16 (1) (2015) 568–571. ISSN 1530–6984.
[2] Caterina Soldano, Ather Mahmood, Erik Dujardin, Production, properties and potential of graphene, Carbon 48 (8) (2010) 2127–2150. ISSN 0008–6223.
[3] Juan Atalaya, Jari M. Kinaret, Andreas Isacsson, Nanomechanical mass measurement using nonlinear response of a graphene membrane, EPL (Europhys. Lett.) 91 (4) (2010) 48001. ISSN 0295–5075.
[4] F. Schedin, A.K. Geim, S.V. Morozov, E.W. Hill, P. Blake, M.I. Katsnelson, K.S. Novoselov, Detection of individual gas molecules adsorbed on graphene, Nat. Mater. 6 (9) (2007) 652–655. ISSN 1476–1122.
[5] Frank Schwierz, Graphene transistors, Nat. Nanotechnol. 5 (7) (2010) 487–496. ISSN 1748–3387.
[6] Changyao Chen, Sunwoo Lee, Vikram V. Deshpande, Gwan-Hyoung Lee, Michael Lekas, Kenneth Shepard, James Hone, Graphene mechanical oscillators with tunable frequency, Nat. Nanotechnol. 8 (12) (2013) 923–927, https://doi.org/10.1038/nnano.2013.232. ISSN 1748-3387.
[7] Konstantin S. Novoselov, V.I. Fal, L. Colombo, P.R. Gellert, M.G. Schwab, K. Kim, A roadmap for graphene, Nature 490 (7419) (2012) 192–200. ISSN 0028–0836.
[8] H. Zhao, K. Min, N.R. Aluru, Size and chirality dependent elastic properties of graphene nanoribbons under uniaxial tension, Nano Lett. 9 (8) (2009) 3012–3015. ISSN 1530–6984.
[9] Axel Eckmann, Alexandre Felten, Artem Mishchenko, Liam Britnell, Ralph Krupke, Kostya S. Novoselov, Cinzia Casiraghi, Probing the nature of defects in graphene by Raman spectroscopy, Nano Lett. 12 (8) (2012) 3925–3930. ISSN 1530–6984.
[10] N. Lindahl, D. Midtvedt, J. Svensson, O.A. Nerushev, N. Lindvall, A. Isacsson, E.E. Campbell, Determination of the bending rigidity of graphene via electrostatic actuation of buckled membranes, Nano Lett. 12 (7) (2012) 3526–3531, https://doi.org/10.1021/nl301080v. ISSN 1530-6992 (Electronic) 1530-6984 (Linking), https://www.ncbi.nlm.nih.gov/pubmed/22708530.
[11] Banafsheh Sajadi, Farbod Alijani, Dejan Davidovikj, Johannes Goosen, Peter G. Steeneken, Fred van Keulen, Experimental characterization of graphene by electrostatic resonance frequency tuning, J. Appl. Phys. 122 (23) (2017a) 234302. ISSN 0021–8979.
[12] Dejan Davidovikj, Farbod Alijani, Santiago J. Cartamil-Bueno, Herre SJ. van der Zant, Marco Amabili, Peter G. Steeneken, Nonlinear dynamic characterization of two-dimensional materials, Nat. Commun. 8.1 (2017), https://doi.org/10.1038/s41467-017-01351-4.
[13] G. López-Polín, M. Jaafar, F. Guinea, R. Roldán, C. Gómez-Navarro, J. Gómez-Herrero, The influence of strain on the elastic constants of graphene, Carbon 124 (2017a) 42–48. ISSN 0008–6223.
[14] R. Nicklow, N. Wakabayashi, H.G. Smith, Lattice dynamics of pyrolytic graphite, Phys. Rev. B 5 (12) (1972) 4951.
[15] Melina K. Blees, Arthur W. Barnard, Peter A. Rose, Samantha P. Roberts, Kathryn L. McGill, Pinshane Y. Huang, Alexander R. Ruyack, Joshua W. Kevek, Bryce Kobrin, David A. Muller, Graphene kirigami, Nature 524 (7564) (2015) 204–207. ISSN 0028–0836.
[16] Yujie Wei, Baoling Wang, Jiangtao Wu, Ronggui Yang, Martin L. Dunn, Bending rigidity and Gaussian bending stiffness of single-layered graphene, Nano Lett. 13 (1) (2012) 26–30. ISSN 1530–6984.
[17] J. Tersoff, Energies of fullerenes, Phys. Rev. B 46 (23) (1992) 15546–15549, https://doi.org/10.1103/PhysRevB.46.15546. ISSN 0163-1829 1095-3795.
[18] Qiang Lu, Marino Arroyo, Rui Huang, Elastic bending modulus of monolayer graphene, J. Phys. Appl. Phys. 42 (10) (2009) 102002. ISSN 0022–3727.
[19] Donald W. Brenner, Olga A. Shenderova, Judith A. Harrison, Steven J. Stuart, Boris Ni, Susan B. Sinnott, A second-generation reactive empirical bond order (rebo) potential energy expression for hydrocarbons, J. Phys. Condens. Matter 14 (4) (2002) 783. ISSN 0953–8984.
[20] Pekka Koskinen, Oleg O Kit, Approximate modeling of spherical membranes, Phys. Rev. B 82 (23) (2010) 235420.
[21] Konstantin N. Kudin, Gustavo E. Scuseria, Boris I. Yakobson, C 2 f, bn, and c nanoshell elasticity from ab initio computations, Phys. Rev. B 64 (23) (2001) 235406.
[22] Wang, Simulations of the bending rigidity of graphene, Phys. Lett. 374 (9) (2010) 1180–1183. ISSN 0375–9601.
[23] Rafael RoldÃ¡n, Annalisa Fasolino, Kostyantyn V. Zakharchenko, Mikhail I. Katsnelson, Suppression of anharmonicities in crystalline membranes by external strain, Phys. Rev. B 83 (17) (2011) 174104.
[24] D.R. Nelson, L. Peliti, Fluctuations in membranes with crystalline and hexatic order, J. Phys. 48 (7) (1987) 1085–1092. ISSN 0302–0738.
[25] Shikai Deng, Vikas Berry, Wrinkled, rippled and crumpled graphene: an overview of formation mechanism, electronic properties, and applications, Mater. Today 19 (4) (2016) 197–212. ISSN 1369–7021.
[26] Wei Gao, Rui Huang, Thermomechanics of monolayer graphene: rippling, thermal expansion and elasticity, J. Mech. Phys. Solid. 66 (2014) 42–58. ISSN 0022–5096.
[27] Wenzhong Bao, Feng Miao, Zhen Chen, Hang Zhang, Wanyoung Jang, Chris Dames, Chun Ning Lau, Controlled ripple texturing of suspended graphene and ultrathin graphite membranes, Nat. Nanotechnol. 4 (9) (2009) 562–566. ISSN 1748–3387.
[28] Ryan JT. Nicholl, Hiram J. Conley, Nickolay V. Lavrik, Ivan Vlassiouk, Yevgeniy S. Puzyrev, Vijayashree Parsi Sreenivas, Sokrates T. Pantelides, Kirill I. Bolotin, The effect of intrinsic crumpling on the mechanics of free-standing graphene, Nat. Commun. 6 (2015).
[29] Duanduan Wan, David R. Nelson, Mark J. Bowick, Thermal stiffening of clamped elastic ribbons, Phys. Rev. B 96 (1) (2017) 014106.
[30] Romain Breitwieser, Yu-Cheng Hu, Yen Cheng Chao, Ren-Jie Li, Yi Ren Tzeng, Lain-Jong Li, Sz-Chian Liou, Keng Ching Lin, Chih Wei Chen, Woei Wu Pai, Flipping nanoscale ripples of free-standing graphene using a scanning tunneling microscope tip, Carbon 77 (2014) 236–243. ISSN 0008–6223.
[31] Gregory W. Vogl, Ali H. Nayfeh, A reduced-order model for electrically actuated clamped circular plates, in: ASME 2003 International Design Engineering Technical Conferences and Computers and Information in Engineering Conference, American Society of Mechanical Engineers, 2003, pp. 1867–1874, https://doi.org/10.1088/0960-1317/15/4/002.
[32] Marco Amabili, Nonlinear Vibrations and Stability of Shells and Plates, Cambridge University Press, 2008, https://doi.org/10.1017/CBO9780511619694. ISBN 1139469029, https://doi.org/10.1017/CBO9780511619694.
[33] Singiresu S. Rao, Vibration of Continuous Systems, John Wiley & Sons, 2007. ISBN 0471771716.
[34] Steve Plimpton, Paul Crozier, Aidan Thompson, Lammps-large-scale atomic/molecular massively parallel simulator, Sandia Nat. Lab. 18 (2007) 43.
[35] R. Klessig, E. Polak, Efficient implementations of the polak–ribière conjugate gradient algorithm, SIAM J. Contr. 10 (3) (1972) 524–549. ISSN 0036–1402.
[36] Denis J. Evans, Brad Lee Holian, The nose–hoover thermostat, J. Chem. Phys. 83 (8) (1985) 4069–4074. ISSN 0021–9606.
[37] Yangfan Hu, Jiapeng Chen, Biao Wang, On the intrinsic ripples and negative thermal expansion of graphene, Carbon 95 (2015) 239–249. ISSN 0008–6223.
[38] Guillermo López-Polín, Maria Ortega, J.G. Vilhena, Irene Alda, J. Gomez-Herrero, Pedro A. Serena, C. Gomez-Navarro, Rubén Pérez, Tailoring the thermal expansion of graphene via controlled defect creation, Carbon 116 (2017b) 670–677. ISSN 0008–6223.
[39] Ali H. Nayfeh, Dean T. Mook, Nonlinear Oscillations, John Wiley & Sons, 2008, https://doi.org/10.1002/9783527617586. ISBN 3527617590.
[40] Banafsheh Sajadi, Farbod Alijani, Hans Goosen, Fred van Keulen, Effect of pressure on nonlinear dynamics and instability of electrically actuated circular micro-plates, Nonlinear Dynam. (2017b) 1–14. ISSN 0924-090X.

[41] Daniel Midtvedt, Alexander Croy, Andreas Isacsson, Zenan Qi, Harold S. Park, Fermi-pasta-ulam physics with nanomechanical graphene resonators: intrinsic relaxation and thermalization from flexural mode coupling, Phys. Rev. Lett. 112 (14) (2014) 145503.
[42] Daniel J. Inman, Engineering Vibration, 2014.
[43] Martin Thomas, Martin Brehm, Reinhold Fligg, Peter Vöhringer, Barbara Kirchner, Computing vibrational spectra from ab initio molecular dynamics, Phys. Chem. Chem. Phys. 15 (18) (2013) 6608–6622.
[44] L. Peliti, S. Leibler, Effects of thermal fluctuations on systems with small surface tension, Phys. Rev. Lett. 54 (15) (1985) 1690.
[45] P. Liu, Y.W. Zhang, Temperature-dependent bending rigidity of graphene, Appl. Phys. Lett. 94 (23) (2009) 231912. ISSN 0003–6951.